Research in Astronomy and Astrophysics, 24:055016 (13pp), 2024 May https://doi.org/10.1088/1674-4527/ad3953

Capture Efficiency Analysis in the Circular Restricted Three-body Problem

Yu-Xuan Miao[1,2,3] and Xi-Yun Hou[1,2,3]
[1] Department of Astronomy and Space Science, Nanjing University, Nanjing 210023, China; houxiyun@nju.edu.cn
[2] Institute of Space Environment and Astrodynamics, Nanjing University, Nanjing 210023, China
[3] Key Laboratory of Modern Astronomy and Astrophysics, Ministry of Education, Nanjing 210023, China
Received 2023 September 11; revised 2024 February 6; accepted 2024 March 22; published 2024 May 10

Abstract

Temporary capture efficiency is studied in the framework of the circular restricted three-body problem in two steps. First, a non-uniform distribution of test particles around the secondary's orbit is obtained by fully accounting the secondary's gravitational influence. Second, the capture efficiency is computed based on the non-uniform distribution. Several factors influencing the result are discussed. By studying the capture efficiency in the circular restricted three-body problem of different mass ratios, a power-law relation between the capture efficiency (p) and the mass ratio (μ) is established, which is given by $p \approx 0.27 \times \mu^{0.53}$, within the range of $3.0035 \times 10^{-6} \leqslant \mu \leqslant 3.0034 \times 10^{-5}$. Taking the Sun–Earth system as an example, the influence from the orbit eccentricity of the secondary on the non-uniform distribution and the capture efficiency is studied. Our studies find that the secondary's orbit eccentricity has a negative influence on the capture efficiency.

Key words: methods: numerical – celestial mechanics – planets and satellites: dynamical evolution and stability

1. Introduction

Gravitational capture is an important dynamical phenomenon in the evolution of the solar system, which has engaged the curiosity of many researchers. It usually occurs when a celestial body approaches a massive planet at a relatively low velocity during a close encounter, leading to a transition from a heliocentric orbit to a planetocentric one (Heppenheimer & Porco 1977). During this process, the orbit may be significantly perturbed from a Keplerian orbit about the Sun as the gravitational perturbation from the close encounter planet becomes dominant.

Hopf (1930) and Tanikawa (1983) demonstrate that the probability of permanent capture in a purely gravitational environment is zero, yet temporary capture is always possible. When combined with some dissipative mechanisms, the temporary capture can become permanent. The dissipative mechanisms can be gas drag (e.g., Hunten 1979; Pollack et al. 1979; Cordeiro et al. 1999; Vieira Neto et al. 2009), a gradual increase in the mass of the central planet (e.g., Heppenheimer & Porco 1977; Vieira Neto et al. 2004), and collisions (e.g., Colombo & Franklin 1971). The capture can also become permanent when a binary asteroid system encounters a planet, in which case one of the bodies is permanently attached to the planet and the other escapes due to the exchange of orbital energies (e.g., Agnor & Hamilton 2006). Due to these mechanisms, the capture process provides researchers with an opportunity to explain the origin and evolution of irregular satellites around four outer solar system planets (e.g., Nesvorný et al. 2007, 2014).

The capture process also arouses interest from the aerospace community as it offers potential fuel savings for interplanetary spacecraft by strategically utilizing the capture mechanism to achieve a nominal orbit around a planet. Belbruno (1987) first proposed the concept of Weak Stability Boundary and successfully applied it to the Japanese Hiten spacecraft (Belbruno & Miller 1993). Topputo & Belbruno (2009), Luo et al. (2014), Luo & Topputo (2017, 2021), Luo (2020) studied the gravity-assisted capture in different systems. Studies have also been carried out on the application of the capture mechanism to retrieve asteroids into the near-Earth space (e.g., Baoyin et al. 2010).

Solving the capture problem analytically is challenging. The capture occurs when celestial bodies encounter the planet at a low relative speed. In such a case, the dynamics are usually chaotic. Murison (1989) and Cordeiro et al. (1999) pointed out the complexity of the capture process in the circular restricted three-body problem (hereafter referred to as CRTBP), since the capture structure in the phase space is partially fractal-like and self-similar. Researchers therefore generally prefer to use numerical methods to study the capture process, and usually make some reasonable assumptions to simplify the situation and reduce the computational difficulty. Carusi & Pozzi (1978), Carusi & Valsecchi (1980) worked on the capture phenomenon of objects located near Jupiter by setting the initial velocities of particles tangential to Jupiter's orbit. Huang & Innanen (1983) studied the stability of retrograde jovicentric orbits to find the relationship between the length of the capture time and the periodic orbits using Henon's diagram (Henon 1970). The mirror theorem (Roy & Ovenden 1955) is also used to simplify the problem whose nature is time reversible and symmetric in the CRTBP. In the study of de Almeida Prado & Vieira Neto

(2006), a polar mesh grid of distance and angle around the capturing planet was adopted. They used the reversibility of time in the CRTBP and integrated the particles backwards until they left the vicinity of the planet. Brunini (1996) explored the capture conditions for particles by placing particles on a fixed line perpendicular to the x-axis. He changed the angle α between the velocity and the x-axis and computed the capture domain in the phase space of (y, α). In addition to these studies, some others also focus on the length of the temporary capture time (e.g., Vieira Neto & Winter 2001; Winter & Vieira Neto 2001; Fedorets et al. 2017). The capture process is also an important part of the transport of matter in interplanetary space. It is the basis for calculating the flux of matter orbiting and impacting the planet.

A practical concern of this study is the computation of the temporary capture efficiency within a general CRTBP system, taking into account the gravitational influence of the secondary (hereafter referred to as P2 and the primary referred to as P1). It represents the probability of a massless particle being temporarily captured by P2 within a prescribed duration. In our work, the capture efficiency serves as a metric for assessing the capability of P2 to capture nearby particles in the CRTBP. The basic method of computing the capture efficiency in our work is the one employed by Granvik et al. (2012) which computes the temporary capture efficiency of near-Earth objects (hereafter referred to as NEOs). It involves the following steps:

1. Choose a ring region enveloping the Earth's orbit. The ring is described by the semimajor axis, orbit eccentricity and inclination, and is discretized by uniformly distributed bins inside it.
2. Inside each bin of the above ring region, generate N_1 random test particles with random values of longitude of the ascending node Ω, argument of periapsis ω, and mean anomaly M in the range of $[0, 2\pi]$;
3. Choose a circumsphere centered at the Earth inside the ring region, and count the number of test particles inside the circumsphere (denoted as N_2);
4. Integrate orbits of the N_2 particles initially inside the circumsphere within a prescribed time T and count the number of particles that are temporary captured by the Earth (denoted as N_3);
5. The capture efficiency of the bin is computed as $p(a, e, i) = N_3/N_1$.

The total capture efficiency of near-Earth objects (NEOs) by the Earth is then obtained by multiplying the orbital element distribution $R(a, e, i)$ of NEOs (Bottke et al. 2002) with the capture efficiency in each bin and then summing over all the bins.

In the current study, we use the same method to compute the capture efficiency, but focus on the general CRTBP model. The orbital element distribution function $R(a, e, i)$ is generated by fully considering the resonance effects between P2 and the particles. Moreover, we made following contributions: (1) A backward integration method is proposed to identify the ring region enveloping the orbit of P2. (2) Influence of the circumsphere size on the capture efficiency is investigated, and appropriate values are recommended. (3) By computing the capture efficiency of CRTBPs with different mass ratios, a power-law relation between the capture efficiency and the mass parameter of CRTBP is established. (4) Influence of P2's orbit eccentricity on the capture efficiency is studied.

The paper is organized as follows. Section 2 is devoted to the methods used in the study, including the way to obtain the non-uniform steady-state distribution which is influenced by the resonances with P2, the way to choose the ring region, the circumsphere size, and the integration time, and the way to compute the capture efficiency. Section 3 presents the main results of our numerical experiments. A power-law relation between the capture efficiency p and the mass ratio μ is given. Section 4 discusses the influence of P2's orbit eccentricity on the capture efficiency. Section 5 concludes the study.

2. Methodology

2.1. Capture Efficiency Computation

The method to compute the capture efficiency is the one used by Granvik et al. (2012), which mainly contains the following steps:

1. The first step is to choose an initial sampling region enveloping P2's orbit. The sampling region is characterized by $[a_{\min}, a_{\max}] \times [e_{\min}, e_{\max}] \times [i_{\min}, i_{\max}]$. It is discretized into a series of bins with uniform step sizes along the semimajor axis, orbit eccentricity, and orbit inclination.
2. Inside each bin, generate a number of test particles whose Ω, ω, and M are randomly distributed within the range of $[0, 2\pi]$. The total number of test particles in each bin is denoted as $M_{\rm gen}$.
3. Choose a circumsphere inside the ring region, with its center at P2. Select test particles that are inside the circumsphere. Denote the number of the selected test particles as $M_{\rm filter}$.
4. Integrate orbits of the selected test particles and count the number of test particles that can be temporarily captured within an integration time δT. Denote the number of captured particles as $M_{\rm cap}$.
5. The capture efficiency of this bin is computed by the following formula:

$$p(a, e, i) = \frac{M_{\rm cap}}{M_{\rm filter}} \frac{M_{\rm filter}}{M_{\rm gen}}. \quad (1)$$

6. Suppose that the distribution of the test particles around P2 is in a steady-state, and is described by a function

$R(a, e, i)$. The total capture efficiency is computed by the following formula:

$$p_{\rm sum} = \iiint p(a, e, i)R(a, e, i)dadedi = \sum_{i=1}^{N_{\rm bin}} p(a, e, i)R(a, e, i) \quad (2)$$

in which $N_{\rm bin}$ is the total number of discretized bins.

In their study, Granvik et al. (2012) used the steady-state distribution of NEOs $R_{\rm NEO}(a, e, i)$ given by Bottke et al. (2002). They also give recommendations of the ring size, circumsphere size and integration time for the Sun–Earth system. However, for the purpose of the current study which focuses on the general CRTBP model, we have to find these settings by ourselves before applying the above method. In the following subsections, we explain more details.

2.2. Capture Criterion and Boundary

The temporary capture criterion is rather a controversial but inevitable issue as there is no precise dynamical constraint on whether a celestial body is captured. Everhart (1973) judged whether a celestial body is captured by monitoring if the osculating planetocentric orbital elements become elliptical. However, Fedorets et al. (2017) mentioned that quasi-satellites may have an osculating orbit eccentricity less than 1 with respect to the planet, while they are not dynamically bound to the planet. Carusi & Pozzi (1978) and Gladman et al. (1995) checked the distance of the particles from the planet. Yamakawa et al. (1992) related the capture efficiency with the two-body energy and assumed that the capture occurs when the energy of the celestial body relative to the planet becomes negative. In Granvik et al. (2012), the same definition as the one used in Kary & Dones (1996) is adopted which includes two criteria:

1. The distance of the celestial body away from P2 is less than three Hill Radii of P2.
2. The two-body Keplerian energy of the celestial body with respect to P2 is less than 0.

Once the particles in the CRTBP system simultaneously satisfy the above two conditions, it can be considered to be temporarily captured by P2. In this study, we take the same two conditions. In the discussion section, we will discuss why we persist using the value of three Hill Radii.

2.3. Initial Sampling Region

One issue to be addressed is how to choose the initial sampling region for a given CRTBP system. Generally, the size of the sampling region should increase with the mass parameter, as the gravitational influence region of P2 expands. We need to specify the initial sampling region in which the gravity of P2 has an obvious influence and the particles have a good chance of being captured (see Figure 1). In this subsection, we propose a backward integration method to identify the initial sampling region.

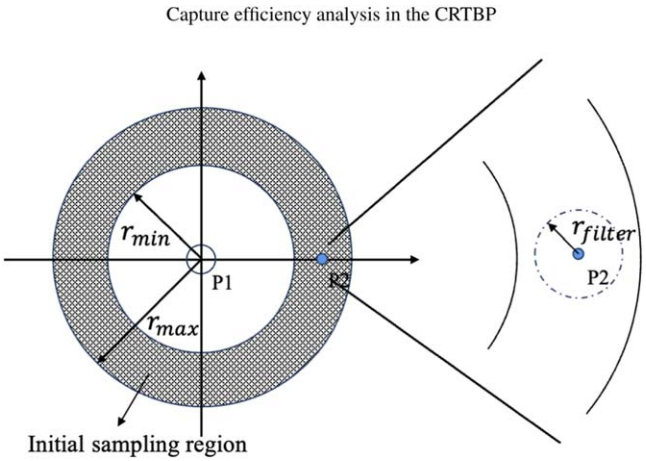

Figure 1. The schematic diagram of the initial sampling region and the circumsphere. The radius $r_{\rm filter}$ corresponds to the radius of the circumsphere and should be inside the initial sampling region. The radius $r_{\rm min}$ and $r_{\rm max}$ represent the inner and the outer boundary of the ring-shaped initial sampling region, which approximately equal the minimum periapsis distance and the maximum apoapsis distance of the particles.

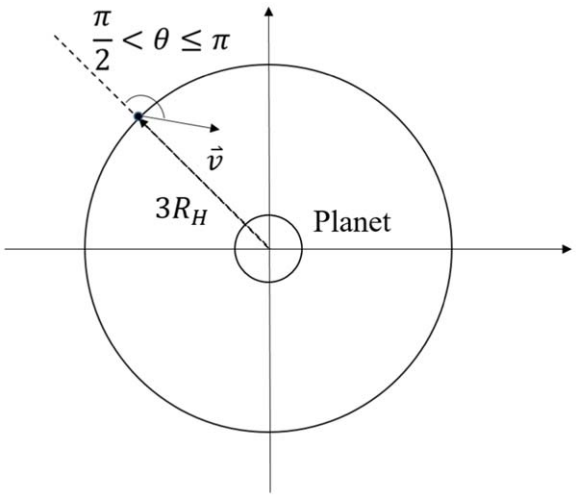

Figure 2. The schematic diagram of the particles being captured and passing the circle with a radius of three Hill Radii of P2. Particles are assumed to have zero energy when they pass through this circle. $\boldsymbol{v}$ is the inbound velocity of the particle at the circle.

A necessary condition for temporary capture is that particles have a low relative velocity at close encounters with P2. This implies that the particles are on orbits characterized by low eccentricities and inclinations with respect to P2 (Qi & Qiao 2023). As a result, we can use the planar CRTBP model

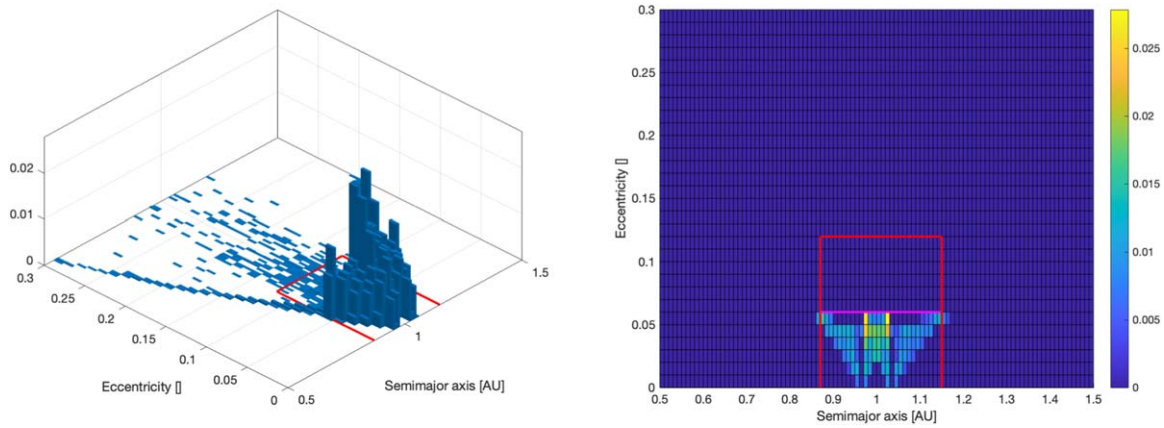

Figure 3. The range of the initial sampling region determined by the backward integration method is shown. The mass parameter is the one of the Sun–Earth system ($\mu_E \approx 3.0035 \times 10^{-6}$). The left frame shows the histogram of the reachable bin in the (a, e) space. The right frame shows the identified initial sampling region (the smaller square) and the one used by Granvik et al. (2012) (the larger square).

to identify the initial sampling region in the (a, e) space. An intuitive idea is that in the planar CRTBP, trajectories of the captured particles should pass through a circle surrounding P2 with an instantaneous incoming velocity $\boldsymbol{v}$ which forms an angle $\theta > \pi/2$ with respect to its position vector, as depicted in Figure 2. By generating points on the circle and performing a backward integration of them from the "capture boundary" (three Hill Radii which is the same as that used in Granvik et al. 2012), we can obtain the region in the space of (a, e) where the particles originate. Since it is possible for the particles to enter the three Hill Radii region at any point on the sphere, the entire circle needs to be surveyed. The energy of the particle with respect to P2 is set to zero as it is also one of the temporary capture criteria used by us. Hence the value of $|\boldsymbol{v}|$ can be solved by this condition.

Using the mass parameter of the Sun–Earth system as an example ($\mu_E \approx 3.0035 \times 10^{-6}$), 100 points are selected uniformly at a distance of three Hill Radii from P2. At each point, we create 100 random directions for the inbound velocity vector $\boldsymbol{v}$ ensuring that the constraint $\theta > \pi/2$ is met. Consequently, there are a total of 100×100 orbits. These orbits are backwards integrated for 100 units of dimensionless time in the CRTBP. For each orbit, we record its minimum and maximum orbit semimajor axes, as well as its maximum orbit eccentricity. The left frame of Figure 3 shows the statistical result. The plane spanned by the semimajor axis and the orbit eccentricity is divided into a series of bins (the resolution is $\Delta a = 0.01$ au, $\Delta e = 0.01$), and the relative weight of each bin is computed by counting the number of particles in it. If we neglect the bins that contain particles less than 10% of the maximum one, we get the initial sampling region (denoted by the smaller square) in the (a, e) space presented in the right frame of Figure 3. The larger square represents the initial sampling region used in Granvik et al. (2012). The two regions agree with each other quite well in the semimajor axis, but not in the orbit eccentricity. The upper boundary of Granvik et al. (2012) is about twice the upper boundary of ours.

Table 1
Parameters Used in the Numerical Experiments

Mass Parameter (μ_E)[a]	a_{min} (au)[b]	a_{max} (au)[b]	e_{max}[b]	N_{bin}[c]	M_{gen}^{tot}[d]	M_{orb}^{tot}[e]
1	0.87	1.15	0.06	840	8.4×10^6	8.4×10^4
2	0.85	1.20	0.08	1400	1.4×10^7	1.4×10^5
3	0.83	1.23	0.09	1800	1.8×10^7	1.8×10^5
4	0.81	1.26	0.10	2250	2.25×10^7	2.25×10^5
5	0.80	1.29	0.11	2695	2.695×10^7	2.695×10^5
6	0.79	1.31	0.12	3120	3.12×10^7	3.12×10^5
7	0.78	1.33	0.12	3300	3.3×10^7	3.3×10^5
8	0.77	1.35	0.13	3770	3.77×10^7	3.77×10^5
9	0.76	1.37	0.14	4270	4.27×10^7	4.27×10^5
10	0.76	1.38	0.14	4340	4.34×10^7	4.34×10^5

Notes.
[a] The mass parameter of the CRTBP systems ($\mu_E \approx 3.0035 \times 10^{-6}$).
[b] The range of the initial sampling region.
[c] The total number of the discretized bins.
[d] The total number of the particles for computing the capture efficiency of each bin.
[e] The total number of the particles for computing the non-uniform steady-state orbit distribution.

With the increase of P2's mass, the size of the initial sampling region also increases. Figure 4 shows the range of initial sampling region when the mass parameter of the system is μ=10μ_E. The range apparently enlarges compared to that in Figure 3. Table 1 lists the relevant parameters used in our work. The bin resolution is set to $\Delta a = 0.01$ au, $\Delta e = 0.01$. As we have mentioned, the capture process mainly happens for planar orbits, so in our study the orbit inclination is restricted as

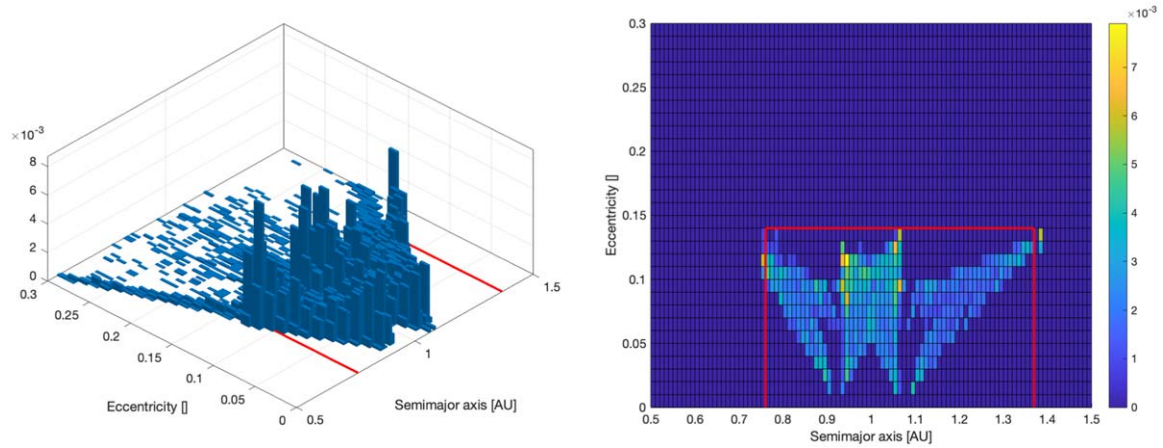

Figure 4. Same as Figure 3 but for a CRTBP with mass parameter of $\mu = 10\mu_E$.

$i \in [0^\circ, 2^\circ.5]$ which is in accordance with Granvik et al. (2012), and the bin size in the orbit inclination direction is $\Delta i = 0.5^\circ. = 0^\circ.5$. We generate 10^4 particles in each bin to compute the capture efficiency $p(a, e, i)$ of this bin.

2.4. Circumsphere Size and Integration Time

It is unnecessary to integrate all the test particles in the initial sampling region. Only test particles close to P2 have a chance to be temporarily captured within a prescribed integration time. Numerically integrating all the test particles is time-inefficient and unnecessary. A clever way to avoid integrating all the test particles is to choose a circumsphere around P2 to filter those that are close to P2 as integration candidates in Granvik et al. (2012). We use the same method in our work. The schematic diagram of the circumsphere is shown in Figure 1. These selected candidates are further integrated for a prescribed time to judge whether they are captured or not. The radius of the circumsphere is denoted as $r_{\rm filter}$ and the length of the integration time is denoted as δT. The final computed capture efficiency p is therefore a function dependent on these two parameters. It is only an approximation of the accurate capture efficiency which should be obtained by integrating all the test particles in the initial sampling region for a long enough integration time.

A natural expectation is that as the circumsphere size increases, the capture efficiency gradually approaches its accurate value. We discretize the circumsphere size in units of Hill Radius of P2 as $r_{\rm filter} = k \cdot R_{\rm H} (k \in \mathbb{N})$. The following relationship should hold:

$$\lim_{k\to\infty} p(k \cdot R_{\rm H}, \delta T) = p(\delta T). \quad (3)$$

For the purpose of practical computation, we need to select an appropriate value of k. One remark is that the circumsphere should be within the initial sampling region. This puts an upper limit for the value of k, denoted as $k_{\rm max}$. For each $k \in [0, k_{\rm max}]$, we compute the capture efficiency $p(k)$. The size selection should be large enough in order not to miss the particles that can be captured during a specific integration time. Starting from smaller values, we select the k value once the following criterion is met:

$$\Delta p(k) = \frac{p(k \cdot R_{\rm H}, \delta T) - p((k-1) \cdot R_{\rm H}, \delta T)}{p((k-1) \cdot R_{\rm H}, \delta T)} \leqslant 10\% \quad (4)$$

where $\Delta p(k)$ stands for the relative increment in capture efficiency for a specific circumsphere size compared to the former one. If the criterion cannot be satisfied unless $k = k_{\rm max}$, we select $k_{\rm max}$ as our k value.

As for the integration time δT, it is obvious that the longer it is, the better the computed result is. However, considering the practical computation cost, we need to put an upper limit to it. In the study of Granvik et al. (2012), the integration time is chosen as 2000 days. In our work, we choose 2 yr for the Sun–Earth system. We will show that the option of this integration time is appropriate.

2.5. Steady-state Orbit Distribution

According to Equation (2), to get the actual capture efficiency, we need a distribution of test particles around P2's orbit. In the work of Granvik et al. (2012), an NEO orbit distribution model $R_{\rm NEO}(a_h, e_h, i_h)$ from Bottke et al. (2002) is utilized. For the general analysis in this study, we do not have the information and we have to generate it by ourselves.

In reality, the distribution of small bodies around a planet's orbit is the result of complicated evolution processes during which the source regions, the gravitational effects, and even some non-gravitational effects (such as collisions and thermal effects) may have their contributions. For the simple CRTBP model considered in this study, P2's gravity is the main contribution for a non-uniform steady-state distribution. It is

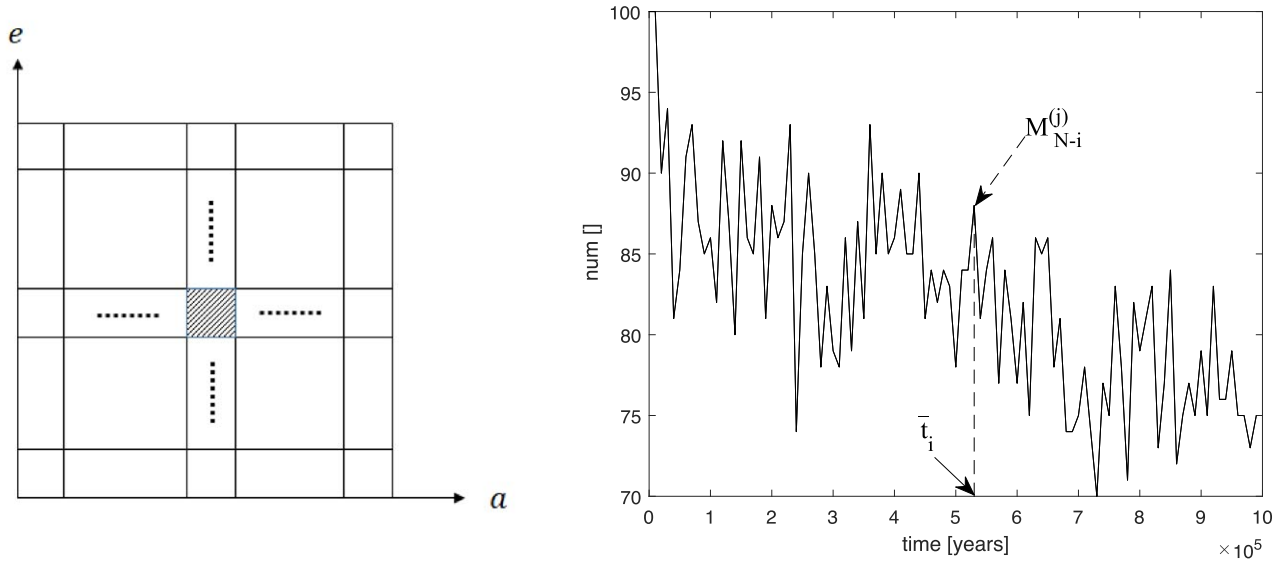

Figure 5. Left frame: One example bin in the two-dimensional phase space spanned by a and e. Right frame: The number of particles in one example bin (ID number is 36) as a function of the evolutionary epoch $\bar{t}_i$.

obvious that due to orbital resonances between P2's orbit and the particles' orbit, the steady-state distribution around P2's orbit is non-uniform. To get the non-uniform orbital element distribution, we start with an initial uniform distribution in the initial sampling region. Take the mass parameter of the Sun–Earth system as an example. The range of this region is $a \in [0.87,\ 1.15]$ au, $e \in [0,\ 0.06]$, $i \in [0^\circ,\ 2^\circ.5]$, and the bin resolution is $\Delta a = 0.01$ au, $\Delta e = 0.01$, $\Delta i = 0^\circ.5$. The angular elements (Ω, ω, M) are uniformly distributed in the range of $[0,\ 2\pi]$.

A time-slicing method is used. The nature of the method is to simulate a dynamically steady-state population by means of time discretization. We assume that the orbital element distribution of the particles around P2's orbit is already in a steady-state. That is to say, influenced by P2's gravity, at any given time, the number of particles leaving the sampling region is equal to the number of particles entering this particular region. At any given observation epoch T and in a specific region of the orbital element space spanned by (a, e, i), we observe the population of the particles. The time is discretized from the initial epoch ($t_0 = 0$) to the epoch T into N equal intervals, so that we have a series of time epochs as $t_i = i \cdot \Delta T$ ($i = 0 \cdots N$) where the time interval $\Delta T = T/N$. The particles observed are a mixture of some old particles that were in this region before epoch T, and some new particles that have just entered this particular region at epoch $t_N = T$.

To simulate this process, we perform the following numerical simulations:

1. Since we are dealing with a continuous system, we first discretize the time into a series of epochs $t_i = i \cdot \Delta T$. The epoch T is the total evolution time and also the observation epoch at which we "observe" the orbital element distribution, and N is the number of time intervals in the total evolution process, i.e., $N = T/\Delta T$. We then divide the phase space of the orbital elements into a set of bins according to certain resolution. Using the two-dimensional phase space spanned by a and e as an example, the left frame of Figure 5 shows one example of the binned orbital element space.
2. At observation epoch T, we count the number of particles in each bin. As we have mentioned, the particles in each bin include those that have only entered the bin at the epoch T, and those that have entered the bin at an earlier epoch $t_i < T$ and still remain in the bin after an evolution interval of $T - t_i$. Denote the number of these particles as $M_i^{(j)}$, where the subscript i is the group number of particles and the subscript j is the ID of the binned orbital element space. The total number of the particles in the bin (j) is therefore $M_i^{(j)} = \sum_{i=0}^{N} M_i^{(j)}$, which is the sum of all previous particles that are in the bin.
3. Suppose that the particles in all bins have an equal chance of evolution. To approximate this equal chance, we give each bin the same number of initial test particles to simulate the initial uniform distribution and track their evolution over time. Starting from the initial epoch $t_0 = 0$, we count the total number of particles from all bins that can enter the bin(j) at each epoch t_i. Of course, the number changes with the epoch t_i. It is necessary to distinguish between the epoch t_i which stands for the group number of particles starting the evolution and the integration epoch which is the evolution time in this

context. If we integrate the test particles for a total time of T and denote the integration time as $\bar{t}_i$, the number at $\bar{t}_i$ corresponds to the particles that have entered the bin at epoch t_{N-i} and remain in the bin after an interval of $T - t_{N-i}$. One example bin is shown in the right frame of Figure 5. According to the curve, it is reasonable to say that the value $M_{N-i}^{(j)}$ at the evolution epoch $\bar{t}_i$ is the number of particles that are in the bin(j) after a time interval of $T - t_{N-i}$. For example, when $i = 0$, the number $M_N^{(j)}$ at epoch $\bar{t}_0$ indicates the initial test particles that have not started their evolution yet, while if $i = N$, the number $M_0^{(j)}$ at epoch $\bar{t}_N$ indicates the final test particles in the bin after an evolution time of T.

The orbital element distribution at the epoch T is thus

$$R(a, e, i, T) = \frac{M^{(j)}(a, e, i)}{M^{\rm tot}}, \quad M^{\rm tot} = \sum M^{(j)}(a, e, i) \quad (5)$$

where $M^{(j)}$ is the total number of the particles at "observation" epoch T in bin(j), and $M_{\rm orb}^{\rm tot}$ is the total number of the particles at "observation" epoch T in all bins. Since a steady-state orbit distribution is assumed, the above process should be independent of the observation epoch T (also the evolution integration time) and $R(a, e, i) = R(a, e, i, T)$. Intuitively, the longer the integration time T, the larger the total number of the test particles for the evolution $M_{\rm orb}^{\rm tot}$, the smaller the time interval ΔT, and the higher the resolution of the bins, the closer the resulting orbital distribution will be to the true case.

In our study, the evolution integration time is set as $T = 10^6$ yr, and the time interval for "observing" the orbit distribution is 10^4 yr. The bin interval is mentioned above as $\Delta a = 0.01$ au, $\Delta e = 0.01$, $\Delta i = 0.^\circ 5$. To carry out the above numerical integration process, we generate 100 particles in each bin to track their orbit evolution. Denote the total number of particles generated to obtain the non-uniform steady-state distribution as $M_{\rm orb}^{\rm tot}$. According to Table 1, within 840 bins, a total of 8.4×10^4 particles are generated. It is necessary to distinguish the number of $M_{\rm orb}^{\rm tot}$ and $M_{\rm gen}^{\rm tot}$ as they correspond to two different numerical processes.

One remark is that the assumption that particles in all bins have an equal chance of evolution is inappropriate. Given that the orbit distribution near P2 is supposed to be in a steady-state and non-uniform, there is no doubt that fewer particles should be in a bin if it has a lower weight $R^{(j)}$, and vice versa. To take this non-uniformity into account, a basic idea is to repeat the above process after obtaining the approximation of the orbital element distribution $R(a, e, i)$ based on the initial uniform distribution. This time, the number of initial particles in each bin for a new evolution process should be chosen according to $R(a, e, i)$, which is also the weight of the bin. However, we did not iterate in this study. In reality, a steady-state distribution is a balance between external sources which keep sending particles into the initial sampling region and the particles that are already in the initial sampling region. Under the sole influence of P2's gravity, the region with a high weight means that orbits of particles in these regions are more stable. On the other hand, particles from external sources are harder to get into these regions due to their stability. As a result, when considering external sources, these regions do not necessarily have a higher weight. Since in our general analysis, we do not have information of external sources, so we prefer not to iterate because otherwise stable regions will gain a higher and higher weight after each iteration. We emphasize that since we only consider P2's gravity in our work, the capture efficiency only reflects the ability of P2 to temporarily capture particles, but is not the real capture efficiency in real physical systems in which real steady-state distribution should be used.

2.6. Numerical Integrators

In our work, two integration algorithms are employed. To compute the non-uniform orbital element distribution introduced in Section 2.5, a hybrid symplectic integrator package, `Mercury6` written by Chambers (1999) is used to compute the dynamical evolution of particles. The hybrid symplectic algorithm can accurately handle close encounters by predicting and using a conventional Bulirsch–Stoer extrapolation integrator to step over it. To compute the capture efficiency, a Runge–Kutta–Felberg 7(8) integrator is used to follow the orbits of the particles within the circumsphere. A particle is removed once it impacts P2 or P1 if its instantaneous P2-centric distance is less than the radius of P2 or its P1-centric distance is less than the radius of P1. The radius of P1 is always assumed to be the same as the Sun, while the radius of P2 increases with mass ratio by keeping the density the same as that of the Earth.

3. Results

In this section, we first take the mass parameter of the Sun–Earth system ($\mu_{\rm E} \approx 3.0035 \times 10^{-6}$) as an example to display the results. After that, the relationship between the capture efficiency p and the mass parameter μ is shown.

3.1. Capture Efficiency of Each Bin

According to Table 1, in each bin 10^4 particles are uniformly generated within the initial sampling region. The range of initial sampling region is: $a \in [0.87,\ 1.15]$ au, $e \in [0,\ 0.06]$, $i \in [0^\circ,\ 2.^\circ 5]$ and the bin resolution is: $\Delta a = 0.01$ au, $\Delta e = 0.01$, $\Delta i = 0.^\circ 5$.

As we have mentioned in Section 2.4, it is necessary to first check the influence of the filtering circumsphere size on the capture efficiency, and choose a proper value for circumsphere size and integration time. Figure 6 displays the capture efficiency for different circumsphere sizes after the integration, as well as the relative increment in the capture efficiency between adjacent two circumsphere sizes defined by

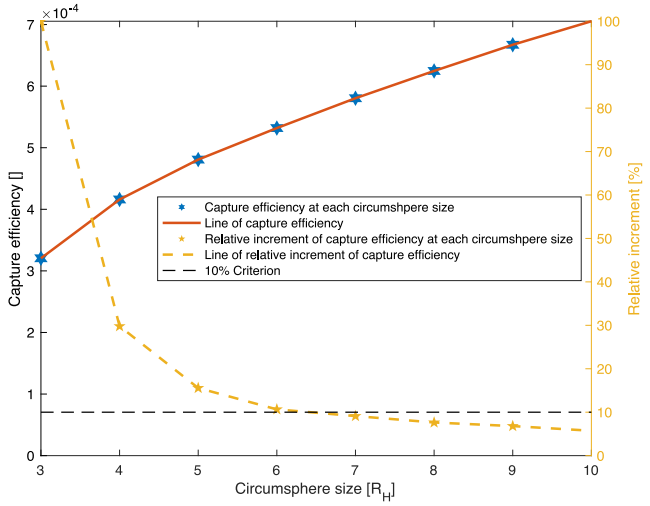

Figure 6. The red line stands for the capture efficiency at each circumsphere size based on the uniform distribution. The yellow line stands for the relative increment in the capture efficiency. The black dashed line is the 10% criterion. At about 7 Hill radii, the relative increment is smaller than 10%.

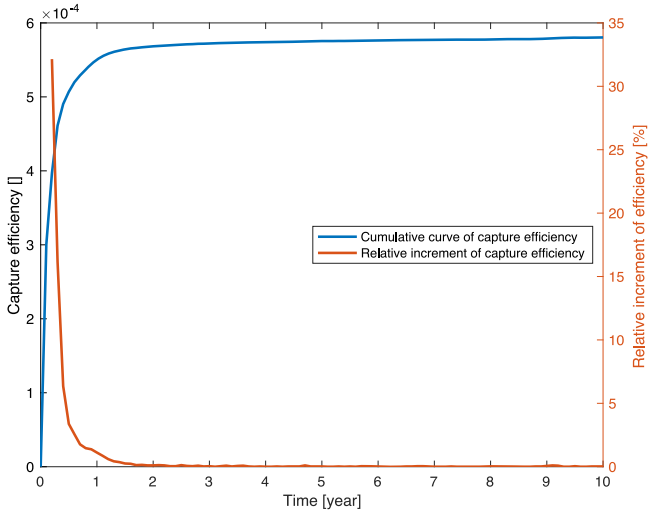

Figure 7. The blue line stands for the cumulative curve of the capture efficiency with respect to the integration time. The red line stands for the relative increment in the capture efficiency. The circumsphere size is set to 7 Hill Radii. After 2 yr of integration, the growth in capture efficiency has almost ceased. A prescribed 2 yr integration time to compute the capture efficiency is long enough.

Equation (4). It seems that when $k = 7$ Hill radii, the relative increment of the capture efficiency is less than 10%. This is larger than the size of the circumsphere taken by Granvik et al. (2012). One remark is that if we set the truncation criterion as 20%, the value of k is around 4–5, which is the value taken by Granvik et al. (2012).

Fixing the circumsphere as seven Hill Radii, Figure 7 shows the relationship between the growth of capture efficiency and the integration time. An obvious trend is that the capture efficiency gradually approaches a fixed critical value when the integration time is long enough. It can be seen that when the particles are integrated for 2 yr, the growth of capture efficiency almost ceases. Therefore, a prescribed 2 yr integration time in the Sun–Earth system is long enough.

Based on the chosen initial sampling region, the circumsphere size, and the integration time, the capture efficiency of each bin can be computed. According to Equation (1), the map of capture efficiency $p(a, e, i)$ in each bin is illustrated in the left frame of Figure 8.

3.2. Steady-state Distribution

To numerically simulate the long-term evolution of the whole population, a total number of 8.4×10^4 particles are integrated for $T = 10^6$ yr, as listed in Table 1. The time interval for observing the state of orbit distribution is $\Delta T = 10^4$ yr. Figure 9 shows the final steady-state distribution of the test particles in the orbital element (a, e) space through the numerical method in Section 3.2. Due to the gravitational influence of P2, the distribution is non-uniform. The bins have a higher weight if the color is lighter. The cumulative ridge in the left frame of Figure 9 is located where the semimajor axis $a = 1$ au. Particles accumulate here because they are on orbits like P2 and are trapped in the 1: 1 resonance. The region with lower weight close to 1 au corresponds to P2-orbit crossers with low orbital eccentricities. Close encounters between P2 and the particles are common here. P2 wipes out the particles here and causes a significant depletion in this region. Particles with semimajor axes further away from 1 au and small orbit eccentricities have little chance to encounter P2, so the bins in this region have a higher distribution weight. When the bin resolution is enhanced to $\Delta a = 0.0005$ au, $\Delta e = 0.0005$ (see the right frame of Figure 9), we can observe some fine structures at specific positions. We believe that these structures are closely related to orbital resonances with P2, which are very close to the 1: 1 one (Pan & Hou 2022; Tan et al. 2023).

According to Equation (2), the capture efficiency $p(a, e, i)$ of each bin is multiplied with the bin weight $R(a, e, i)$. The result is illustrated in the right frame of Figure 8. Based on the non-uniform steady-state distribution and the capture efficiency of each bin, the capture efficiency is computed as $\sim 2.930 \times 10^{-4}$, which is only $\sim$50.49% of the value if using a uniform steady-state distribution.

3.3. Relationship between the Capture Efficiency and the Mass Ratio

In this section, we study the relation between the capture efficiency p and the mass ratio μ. The values of the mass parameters are listed in Table 1 and the corresponding capture

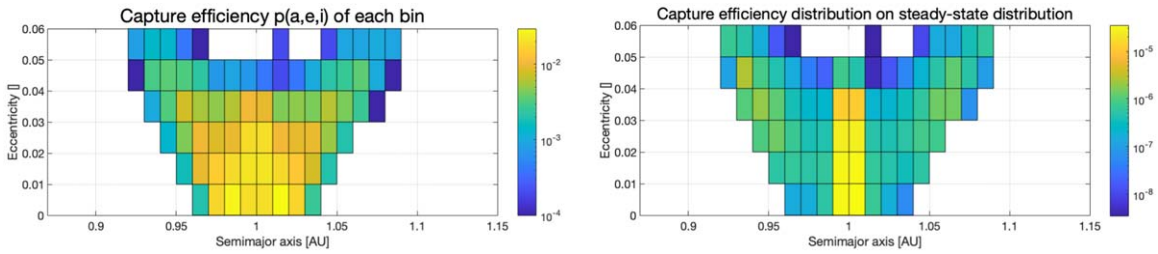

Figure 8. The left frame is the capture efficiency $p(a, e, i)$ of each bin for a mass parameter of the Sun–Earth system. The right frame is the modified capture efficiency distribution based on the non-uniform steady-state distribution. The colorbar means the capture efficiency of the bin.

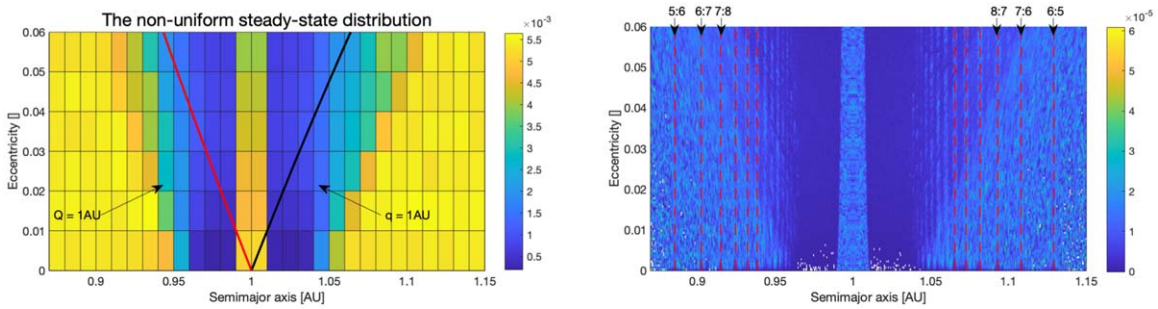

Figure 9. The steady-state distribution of the particles near P2's orbit for the system with $\mu \approx 3.0035 \times 10^{-6}$. The colorbar is the relative weight of the bin. (1) The left frame: The distribution in the (a, e) space with the bin resolution as $\Delta a = 0.01$ au, $\Delta e = 0.01$. The red line stands for test particles with apoapsis distance of 1 au and the black one stands for test particles with periapsis distance of 1 au; (2) The right frame: The distribution in the (a, e) space with the resolution as $\Delta a = 0.0005$ au, $\Delta e = 0.0005$. The red dashed lines stand for the positions of the orbital resonances with P2, which match the computed fine structures well.

efficiency values are computed. The procedure of computing the capture efficiency for different mass ratios μ is the same as that for the Sun–Earth system described in Sections 3.1 and 3.2. The sizes of the initial sampling regions and the total numbers of test particles used in the numerical simulations are also listed in Table 1. The results of the capture efficiency for different mass ratios based on different orbit distributions are displayed in Figure 10. The red dots and fitted short-dash line correspond to the results of the uniform steady-state distribution of test particles, i.e., P2's gravitational influence on the orbital element distribution is ignored. The green dots and fitted dotted–dashed line correspond to the results of the non-uniform distribution of test particles, which is obtained by fully considering P2's gravitational influence. Obviously, the capture efficiency of the non-uniform distribution is smaller than the result of assuming a uniform distribution. For the non-uniform steady-state which considers the gravitational influence of P2, a power-law relation between the capture efficiency p and the mass ratio μ is fitted as

$$p \approx 0.27 \times \mu^{0.53}$$

in which $3.0035 \times 10^{-6} \leqslant \mu \leqslant 3.0034 \times 10^{-5}$.

4. Discussion

4.1. Capture Boundary

In Section 2.2, if we refer to the P2-centric distance in Criterion 1 as "capture boundary", it is natural to wonder whether the final computed result would be significantly changed when this value is altered. In previous work, Granvik et al. (2012) and Kary & Dones (1996) did not explain the reason why three Hill Radii is chosen as the boundary to judge whether a particle is captured by the planet. Intuitively, the farther the particles are away from the planet, the lower the probability that their Keplerian energy becomes negative.

In order to investigate the influence of the capture boundary on the computed capture efficiency and to justify the plausibility of using three Hill Radii, we integrate all the particles within the circumsphere (seven Hill Radii) around P2 for $\delta T = 2$ yr. During the integration process for each particle, when the Keplerian energy is less than 0, the minimum distance of the particle from P2 is recorded. That is to say, particles with minimum distance from P2 less than three Hill Radii are precisely those that can be captured when the capture boundary is set to three Hill Radii. The distribution of particles' minimum distances from P2 is displayed in Figure 11. According to the cumulative capture efficiency curve, it is evident that the

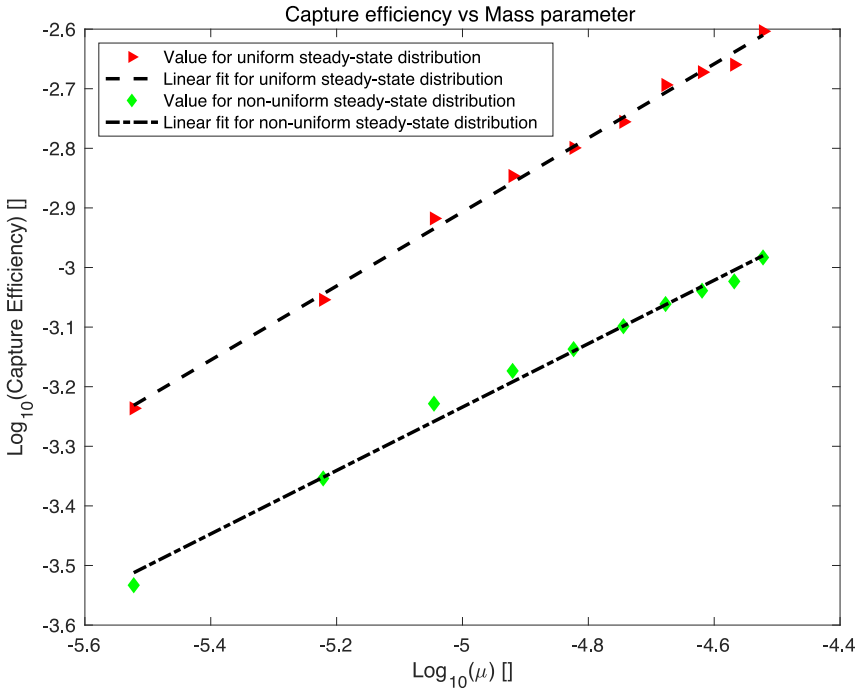

Figure 10. Linear fit for relation between $\log_{10}(\mu)$ and $\log_{10}(p)$ based on uniform and non-uniform steady-state distributions.

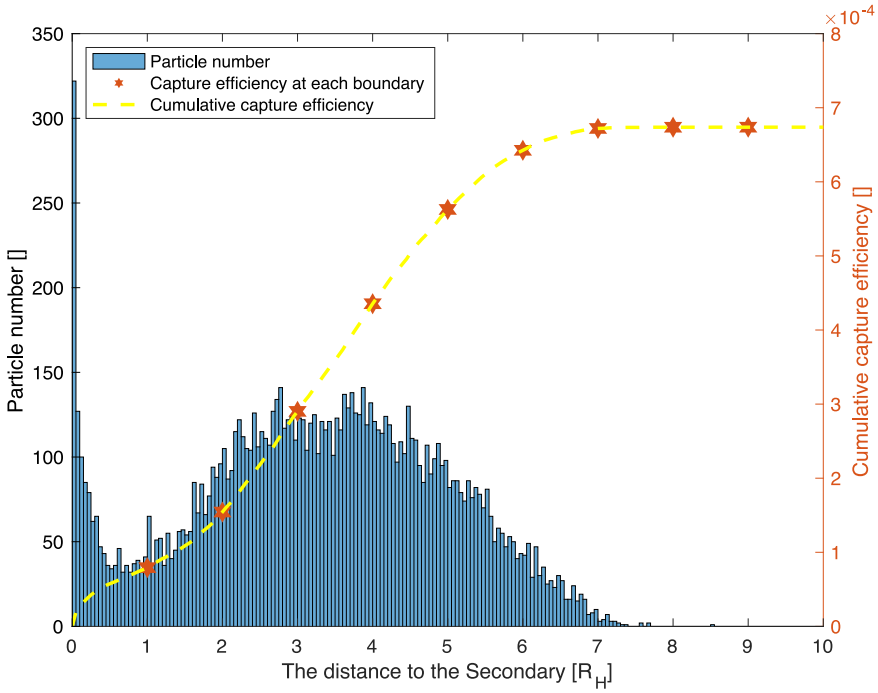

Figure 11. The minimum distance from P2 for test particles with a negative Keplerian energy during the 2 yr integration. The histogram stands for the particle number. The yellow dashed line stands for the cumulative capture efficiency based on a uniform steady-state distribution assumption. The red hexagons are the capture efficiency based on the uniform steady-state distribution at specific capture boundary values ranging from one to ten Hill Radii of P2.

capture efficiency increases as the capture boundary increases. Within one Hill Radius from P2, the number of particles decreases as the distance from P2 increases. This implies that particles have a higher likelihood of being found near P2 after entering the Hill Radius. Another peak in the distribution of the minimum distances of particles from P2 occurs around three to four Hill Radii. From an alternative perspective, when P2-centric distance is beyond one Hill Radius, particles with negative energy are more likely to be found in the range of 3–4 Hill Radii. This may help explain why a three Hill Radii capture boundary serves as a choice for truncation of capture process.

4.2. Orbit Eccentricity of P2

The majority of our work is conducted under the framework of CRTBP model. The relative geometry between P1 and P2 remains constant over time. The long-term gravitational influence of P2 can thus be investigated and the relationship between the capture efficiency and the mass parameter can be established only by altering the mass parameter. In the real context, planetary orbits are typically elliptic. In this subsection, we extend our work to the elliptic restricted three-body problem (ERTBP) and alter the orbit eccentricity of P2 to examine whether it would influence the capture efficiency or not.

The system used here is also the one with a mass parameter of the Sun–Earth CRTBP system. The orbit eccentricities of P2 are listed in Table 2 as 0, 0.0167 (Earth-like orbit), 0.05 and 0.1. The first thing is to determine the initial sampling region when the P2's orbit eccentricity is non-zero. The same backward integration method in Section 2.3 is used both at periapsis and apoapsis of P2's orbit. Our studies indicate that the size of the initial sampling region increases with P2's orbit eccentricity. For the case of P2's orbit eccentricity equals 0.1, the initial sampling region is identified as: $a \in [0.78, 1.28]$ au, $e \in [0, 0.17]$, $i \in [0°, 2.°5]$. In order to compare the capture efficiency of different orbit eccentricity values at the same condition, we set the initial sampling region for all the tested orbit eccentricities as this one, and the bin resolution is: $\Delta a = 0.01$ au, $\Delta e = 0.01$, $\Delta i = 0.°5$.

Basically, the same method as above has been used to compute the capture efficiency of each bin and the steady-state distribution. Considering that the relative geometry of ERTBP changes as P2 revolves around P1, an additional epoch is assigned to the particles during their generation. The epoch is uniformly distributed in the range of $[0, 2\pi]$ to average over the geometry between the particle, P2 and P1. Figure 12 displays the capture efficiency $p(a, e, i)$ of each bin for different orbit eccentricity values. An obvious fact is that the center of the map remains close to the orbit eccentricity of P2. According to Table 2, the total capture efficiency decreases as the orbit eccentricity of P2 increases. This indicates that P2's orbit eccentricity has a negative influence on the total capture efficiency. It is noticeable that the capture efficiency for orbit eccentricity of P2 to be 0 in Figure 12 differs from the one computed in Section 3.2. This discrepancy is due to the fact that a larger initial sampling region is used here. It has been mentioned in Section 1 that the capture efficiency in our work serves as an indicator of P2's ability to capture nearby particles within a specific region. The computed result is dependent on the choice of the initial sampling region and the alteration of the sampling region here is solely for the purpose of discussing the potential impact of P2's orbit eccentricity on the capture efficiency.

5. Conclusion

In this paper, we study the temporary capture efficiency of massless particles around P2's orbit in the framework of CRTBP. We focus on the gravitational influence of P2 on the capture efficiency. The final computed capture efficiency based on the non-uniform steady-state distribution which fully takes P2's gravity into account is different from the one based on the uniform steady-state distribution. In the Sun–Earth CRTBP system ($\mu_{\rm E} \approx 3.0035 \times 10^{-6}$), the capture efficiency based on the non-uniform distribution is computed as $\sim 2.930 \times 10^{-4}$. In this case, the initial sampling region which envelops P2's orbit is given as $a \in [0.87, 1.15]$ au, $e \in [0, 0.06]$, $i \in [0°, 2.°5]$. The circumsphere size is set to 7 Hill Radii of P2.

The way to compute the capture efficiency is the one used in Granvik et al. (2012). The relevant physical parameters during the process are also investigated and some reference values are recommended. A backward integration method is proposed to identify the initial sampling region. The circumsphere size around P2 is also altered to choose a proper value. With the relative increment in capture efficiency at specific circumsphere size less than 10%, 7 Hill Radii of P2 is recommended as the circumsphere size in the Sun–Earth CRTBP system. A 2 yr integration time is demonstrated to be long enough to compute the capture efficiency. Furthermore, we also find a power-law relation between the capture efficiency and mass parameter, which holds as

$$p \approx 0.27 \times \mu^{0.53}$$

when $3.0035 \times 10^{-6} \leqslant \mu \leqslant 3.0034 \times 10^{-5}$.

It is emphasized that since we do not consider realistic orbit element distributions of small bodies around the planet, the capture efficiency computed is not the real one of the planet, but it can serve as a metric for assessing the planet's capability to capture nearby particles within a specific region. We believe that the planet's gravity is a dominant factor which influences the steady-state distribution and the capture efficiency. The time-slicing method enables us to generate a steady-state distribution of nearby particles for a given planet. Moreover, although the algorithm is basically the same one taken by

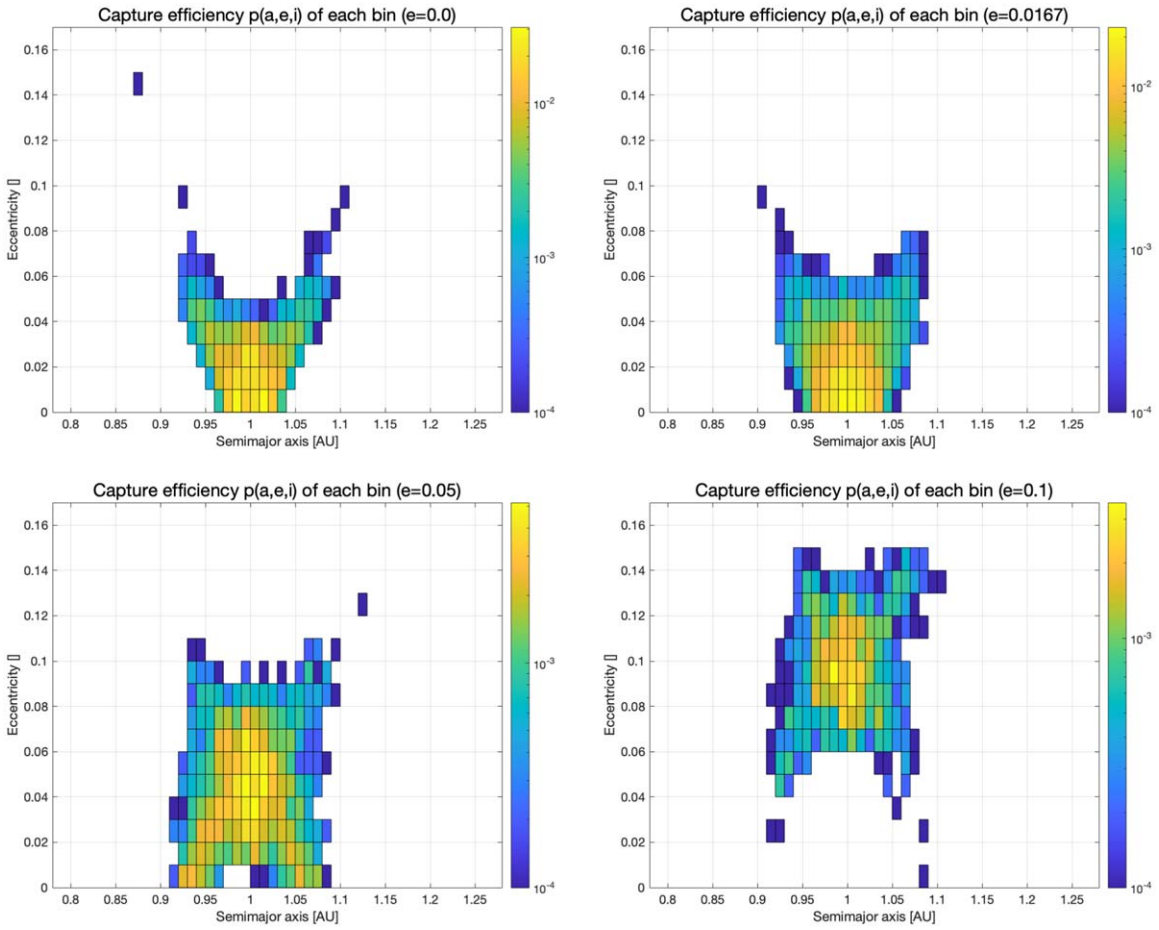

Figure 12. Capture efficiency $p(a, e, i)$ of each bin in the initial sampling region for different values of P2's orbit eccentricity. The initial sampling region is $a \in [0.78, 1.28]$ au, $e \in [0, 0.17]$, $i \in [0^\circ, 2^\circ.5]$ and the bin resolution remains: $\Delta a = 0.01$ au, $\Delta e = 0.01$, $\Delta i = 0^\circ.5$. The orbit eccentricities of P2 are: (1) Upper left: $e = 0$; (2) Upper right: $e = 0.0167$ (Earth-like orbit); (3) Lower left: $e = 0.05$; (4) Lower right: $e = 0.1$. The colorbar means the capture efficiency in the bin.

Table 2
Test Values of the ERTBP's Orbit Eccentricity, Along with the Total Capture Efficiency

Orbit Eccentricity	0	0.0167	0.05	0.1
p	5.928×10^{-5}	4.931×10^{-5}	2.142×10^{-5}	1.195×10^{-5}

Granvik et al. (2012), the ways to choose parameters of the algorithm such as the size of the initial sampling region, circumsphere size and integration time can serve as good references if one wants to study the capture efficiency of some particular planet once a reliable orbit element distribution around it is available. The power-law relation between the capture efficiency and the mass parameter provides us with a quick reference of capture capability for any planets within the specific range ($\mu_E \leqslant \mu \leqslant 10\mu_E$). To be more realistic, we extend our work to the ERTBP. When the orbit eccentricity of P2 increases, the computed capture efficiency decreases. This means that the orbit eccentricity of P2 has a negative influence on the capture efficiency.

Our next step is to analyze the capture efficiency in the case where dissipative forces such as the Poynting–Robertson drag and the Yarkovsky effect are included. These thermal forces are significant for celestial bodies with small sizes. We try to find out how these thermal forces along with the gravity of P2 can affect the capture efficiency of particles in the vicinity. This may help us better understand the role of dissipative forces in the evolutionary history of small celestial objects around the planet, e.g., dust particles around Earth's orbit.

Acknowledgments

This work is supported by the National Natural Science Foundation of China (No. 12233003). X.Y.H. thanks the support from Laboratory of Pinghu, Pinghu, China.

Data Availability

The data that support the findings of this study are available from the author upon reasonable request.

References

Agnor, C. B., & Hamilton, D. P. 2006, Natur, 441, 192
Baoyin, H.-X., Chen, Y., & Li, J.-F. 2010, RAA, 10, 587
Belbruno, E. 1987, in 19th Int. Electric Propulsion Conf. *(Colorado Springs, CO)* (AIAA, DGLR, and JSASS), 1054
Belbruno, E. A., & Miller, J. K. 1993, JGCD, 16, 770
Bottke, W. F., Morbidelli, A., Jedicke, R., et al. 2002, Icar, 156, 399
Brunini, A. 1996, CeMDA, 64, 79
Carusi, A., & Pozzi, F. 1978, M&P, 19, 71
Carusi, A., & Valsecchi, G. B. 1980, M&P, 22, 113
Chambers, J. E. 1999, MNRAS, 304, 793
Colombo, G., & Franklin, F. A. 1971, Icar, 15, 186
Cordeiro, R. R., Martins, R. V., & Leonel, E. D. 1999, AJ, 117, 1634
de Almeida Prado, A. F. B., & Vieira Neto, E. 2006, JAnSc, 54, 567
Everhart, E. 1973, AJ, 78, 316
Fedorets, G., Granvik, M., & Jedicke, R. 2017, Icar, 285, 83
Gladman, B. J., Burns, J. A., Duncan, M. J., & Levison, H. F. 1995, Icar, 118, 302
Granvik, M., Vaubaillon, J., & Jedicke, R. 2012, Icar, 218, 262
Henon, M. 1970, A&A, 9, 24
Heppenheimer, T. A., & Porco, C. 1977, Icar, 30, 385
Hopf, E. 1930, MatAn, 103, 710
Huang, T. Y., & Innanen, K. A. 1983, AJ, 88, 1537
Hunten, D. M. 1979, Icar, 37, 113
Kary, D. M., & Dones, L. 1996, Icar, 121, 207
Luo, Z.-F. 2020, MNRAS, 498, 1515
Luo, Z. F., & Topputo, F. 2017, CNSNS, 48, 211
Luo, Z.-F., & Topputo, F. 2021, AsDyn, 5, 167
Luo, Z. F., Topputo, F., Bernelli-Zazzera, F., & Tang, G. J. 2014, CeMDA, 120, 433
Murison, M. A. 1989, AJ, 98, 2346
Nesvorný, D., Vokrouhlický, D., & Deienno, R. 2014, ApJ, 784, 22
Nesvorný, D., Vokrouhlický, D., & Morbidelli, A. 2007, AJ, 133, 1962
Pan, S., & Hou, X. 2022, RAA, 22, 072002
Pollack, J. B., Burns, J. A., & Tauber, M. E. 1979, Icar, 37, 587
Qi, Y., & Qiao, D. 2023, AsDyn, 7, 3
Roy, A. E., & Ovenden, M. W. 1955, MNRAS, 115, 296
Tan, P., Hou, X.-y., & Liao, X.-h. 2023, MNRAS, 522, 2821
Tanikawa, K. 1983, CeMec, 29, 367
Topputo, F., & Belbruno, E. 2009, CeMDA, 105, 3
Vieira Neto, E., & Winter, O. C. 2001, AJ, 122, 440
Vieira Neto, E., & Winter, O. C. 2009, Math. Probl. Eng., 2009, 897570
Vieira Neto, E., Winter, O. C., & Yokoyama, T. 2004, A&A, 414, 727
Winter, O. C., & Vieira Neto, E. 2001, A&A, 377, 1119
Yamakawa, H., Kawaguchi, J., Ishii, N., & Matsuo, H. 1992, in Proc. of the 2nd AAS/AIAA Meeting *(Spaceflight Mechanics 1992)* ed. R. E. Diehl et al. (San Diego, CA: Univelt), 1113